Ultimate Passivity

Balancing Performance and Stability in Physical Human-Robot Interaction

Guo, Xinliang; Liu, Zheyu; Crocher, Vincent; Tan, Ying; Oetomo, Denny; Stienen, Arno H.A.

DOI
10.1109/TRO.2025.3546856

Publication date
2025

Document Version
Final published version

Published in
IEEE Transactions on Robotics

Citation (APA)
Guo, X., Liu, Z., Crocher, V., Tan, Y., Oetomo, D., & Stienen, A. H. A. (2025). Ultimate Passivity: Balancing Performance and Stability in Physical Human-Robot Interaction. *IEEE Transactions on Robotics*, *41*, 2050-2066. https://doi.org/10.1109/TRO.2025.3546856

Ultimate Passivity: Balancing Performance and Stability in Physical Human–Robot Interaction

Xinliang Guo, *Student Member, IEEE*, Zheyu Liu, Vincent Crocher, Ying Tan, *Fellow, IEEE*, Denny Oetomo, *Senior Member, IEEE*, and Arno H. A. Stienen

***Abstract*—Haptic interaction is critical in physical human–robot Interaction (pHRI), given its wide applications in manufacturing, medical and healthcare, and various industry tasks. A stable haptic interface is always needed while the human operator interacts with the robot. Passivity-based approaches have been widely utilized in the control design as a sufficient condition for stability. However, it is a conservative approach which therefore sacrifices performance to maintain stability. This article proposes a novel concept to characterize an ultimately passive system, which can achieve the boundedness of the energy in the steady-state. A so-called ultimately passive controller (UPC) is then proposed. This algorithm switches the system between a nominal mode for keeping desired performance and a conservative mode when needed to remain stable. An experimental evaluation on two robotic systems, one admittance-based and one impedance-based, demonstrates the potential interest of the proposed framework compared to existing approaches. The results demonstrate the possibility of UPC in finding a more aggressive tradeoff between haptic performance and system stability, while still providing a stability guarantee.**

***Index Terms*—Haptic interface, passivity, physical human–robot interaction (pHRI), ultimately passive controller (UPC).**

I. Introduction

HAPTIC systems, and more generally physical human–robot Interaction (pHRI), constitute a subclass of robotic systems aimed to directly and physically interact with a human operator. Such systems are used in many applications, including surgical robotics [1], haptic exploration [2], robot-assisted rehabilitation [3], and manufacturing and smart assembly [4]. In all its applications, the pHRI system needs to ensure a stable and safe interaction while being able to render the desired physical behavior. The systems generally rely on an impedance control formulation [5] which aims to regulate the interaction between the haptic interface and its environment, including the human operator. These can either be an impedance device, which measures the resulting user displacement and regulates the interaction force, or an admittance device [6], which measures the interaction force and regulates the position (or velocity) of the system. In both cases, the stability of the haptic interaction is critical for both robots and human operators in preventing undesired or dangerous behaviors which might be caused by unstable response of the robot. This stability often comes as a compromise to the haptic interface performance which is required to render an arbitrary virtual environment (VE). There thus exists a challenge to appropriately balance the performance and the stability of the interaction.

One approach to address this problem consists of modeling the entire interaction, which includes the human operator. Doing such modeling allows to evaluate the stability of the entire coupled system, and to design only appropriate VEs to ensure stability. For example, the impedance of the human end-point was modelled as a 2nd-order linear time-invariant (LTI) system as an estimate of the human effect [6], [7]. However, obtaining accurate models for highly nonlinear human behavior is challenging and the robot information necessary for the modelling exercise is not always available to users.

Alternatively, passivity-based approaches have been widely adopted to address this problem due to their ease of implementation where no model information about the environment is required [8]. Given that passivity is a sufficient condition to ensure stability and that the coupling of passive systems is itself passive, this ensures stability under the assumption that the human operator is also passive. However, passivity is a conservative method to guarantee stability [9], which inherently compromises the system performance. While studies [10], [11], [12] have aimed to relax passivity constraints, some knowledge of the environment (i.e., human model) is necessary for alternative stability analyses. This requirement, in return, offsets the ease of use offered by passivity-based approaches. Therefore, when leveraging the passivity concept for practicality, designing a haptic interface satisfying stability while allowing high fidelity rendering of the VE remains challenging.

A. Related Work

Multiple passivity-based approaches have been presented and evaluated in the literature in the past decades. While presenting

Received 14 November 2024; accepted 26 January 2025. Date of publication 28 February 2025; date of current version 21 March 2025. The work was supported in part by the Australian Research Council's Linkage Projects funding scheme under Grant LP180101074. This article was recommended for publication by Associate Editor A. Cherubini and Editor K. Mombaur upon evaluation of the reviewers' comments. *(Corresponding author: Xinliang Guo.)*

Xinliang Guo, Zheyu Liu, Vincent Crocher, Ying Tan, and Denny Oetomo are with the Human Robotics Laboratory, Department of Mechanical Engineering, The University of Melbourne, Parkville, VIC 3010, Australia (e-mail: xinliangg@student.unimelb.edu.au; zheyul@student.unimelb.edu.au; vcrocher@unimelb.edu.au; yingt@unimelb.edu.au; doetomo@unimelb.edu.au).

Arno H. A. Stienen is with the Department of BioMechanical Engineering, Faculty of Mechanical Engineering, The Delft University of Technology, 2628 CD Delft, The Netherlands (e-mail: a.h.a.stienen@tudelft.nl).

This article has supplementary downloadable material available at https://doi.org/10.1109/TRO.2025.3546856, provided by the authors.

Digital Object Identifier 10.1109/TRO.2025.3546856

some differences (see below), all these approaches rely on a measure (or observation) of the energy of the system and attempt to maintain that energy positive at all time.

1) Early Work: In the context of pHRI, time-domain passivity algorithm was introduced in [13] and further elaborated in [14]. This algorithm is the foundation of most approaches developed afterwards. It is implemented as a Passivity Observer (PO) which computes in real-time the amount of energy of the system by measuring its input(s) and output(s). When the energy observed is about to become negative, a Passivity Controller (PC) modifies the rendered impedance (or admittance) to dissipate the required amount of excess energy (typically in the form of a virtual damper). Doing so the energy generated in the system can be dissipated at all time, and the passivity–and so the stability–can be ensured. This approach (referred to as "classic PO-PC") tends to provide an average suboptimal performance–understood as the fidelity of the effectively rendered VE–at all times, without control on when the energy is dissipated (and the performance altered).

2) Bounding Outputs Approaches: Unlike classic PO-PC in which a PC takes actions to dissipate the excess energy only after the PO observes it, some approaches have attempted to modulate (compromise) the original desired performance–corresponding to the desired reference position or force signals to be executed by the robot controller–to prevent violating the passivity condition. One example is the Passive-Set-Position-Modulation framework [15], which was proposed to preserve passivity in the scenario of slowly updating discrete set-position signals (desired positions) of an impedance trajectory-tracking robot where too large virtual springs would otherwise lead to unpassive behaviors. This approach modulates the desired position to be as close as possible to the original set-position signal, but only to the extent determined by the system's available energy to ensure the system is always passive.

Another representation of such reference modulation based methods is the force bounding approach (FBA). FBA maintains passivity by saturating the desired controller force (defined by VE) below a bound determined by the total accumulated energy in the system [16]. A more conservative sufficient passivity condition of FBA was also proposed to systematically remove the past accumulated dissipation capability [17] and so avoid the unwanted oscillations caused by the memory effect. However, as a compromise, adopting this more conservative condition leads to a potentially lower bound of permissible controller force and so more heavily sacrificed performance. A more recent FBA study [18] extended the passivity condition to involve relative motion between moving virtual objects and a human operator, so that stable interaction can be guaranteed even if the VE is dynamic.

Energy Bounding Approach (EBA) is another example of bounding outputs, where the VE's permissible impedance range is bounded, and the desired controller force is adapted accordingly [19]. This displayable impedance range of VE is defined by the energy dissipation capability of the haptic interface (i.e. its effective damping element) so that passivity is always ensured. Given the intrinsically conservative nature of EBA, a subsequent study [20] provided a way to relax EBA constraints, allowing some transient periods with a larger permissible impedance range. Still, when rendering an arbitrary VE, EBA might cause a significant loss of performance to preserve passivity at all time.

3) Energy Tank Approaches: All above approaches keep track of the current energy in the system in order to guarantee passivity but without explicitly referring to such accumulation as an "energy tank" (using the terms "energy reservoir" [15] or "(accumulated) dissipation capability" [17], [19]). Energy-tank approaches differentiate themselves by defining explicit policies as to when to spend the accumulated energy. The tank stores the energy dissipated by the system as an energy margin, which can be used to implement energy-demanding actions (i.e., rendering varying stiffness of VE with an impedance device) when needed while preserving passivity [21], [22], [23], [24].

A recent implementation leverages the energy tank idea together with a robot oscillation detector to stabilize the interaction [25]. This approach proved efficient for pHRI using admittance devices.

4) Two-Layer Approaches: Leveraging the strength of energy tank, a two-layer approach was proposed for passive bilateral telemanipulation [26], [27], [28], [29]. This two-layer hierarchy includes a top layer for implementing desired performance and a bottom layer for enforcing passivity. If the desired torque from the top layer exceeds the maximum allowable torque (determined by the energy tank level), the bottom layer saturates the controller torque to prevent a loss of passivity. Given that these two layers work and communicate separately, this control hierarchy is particularly beneficial to bilateral telemanipulation as performance can be improved (almost) independently on the master and slave sides [26].

B. Contribution

Although passivity-based approaches are relatively straightforward to implement, their inherently conservative nature might lead to the persistent intermittent sacrifice of desired performance as a tradeoff for preserving passivity. However, for some applications, it might be desirable to tie the performance to human behavior instead. One can choose to sacrifice performance more heavily at a given time when the human operator is less compliant and to keep a better performance at all other times. In the case of haptic rendering with an impedance device [30], [31], clearly sacrificing performance (i.e., the rendered stiffness) at one given instant (and notifying the user) instead of regularly mildly affecting it provides a more accurate rendering of the VE. Rehabilitation using an admittance device is another example of application: when the human exhibits high impedance (i.e., high stiffness due to a spastic reaction or hypertonicity), there is little interest in highly enforcing the expected transparent behavior. It is then desirable to stabilize the system and accumulate excess energy at a given time to allow an average better performance afterwards. Therefore, these ideal tradeoffs between stability and performance are still to be defined and implemented for specific applications.

This article thus proposes the concept of "ultimate passivity"—a novel approach that ensures passivity in steady-state while allowing nonpassive behaviors during transient

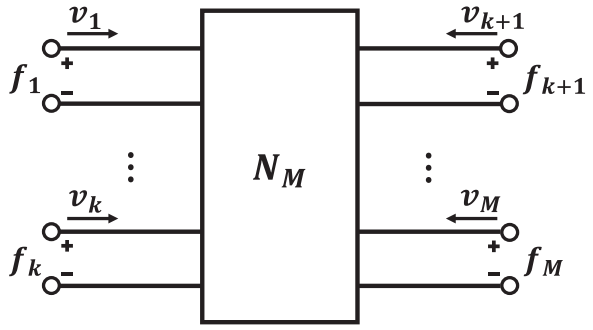

Fig. 1. M-port network model diagram [13].

phases. Such a concept takes advantage of the idea of classic PO-PC [14] and energy tank [25] by accumulating energy when performance may be sacrificed to spend it subsequently to obtain a more desirable performance at all other times. However, different from all other strategies as summarized in Section I-A, the ultimate passivity approach allows bounded nonpassive transients while guaranteeing that the system will ultimately return to a passive state. Such approach provides higher flexibility in defining the tradeoff between stability and performance. Specifically, by changing the PC's configuration, it allows to determine how often and how quickly the PC sacrifices the rendering performance to ensure that the system is ultimately passive based on the application need.

The rest of this article is organized as follows. Section II introduces the ultimate passivity concept, Section III defines the exact problem formulation, and Section IV proposes an implementation framework of ultimately passive controller (UPC) and provides sufficient conditions to ensure the overall system is ultimately passive. An experimental evaluation on an admittance-based robot is presented in Section V to compare the performance of the proposed UPC with the state of the art. Such evaluation is also performed on an impedance-based robotic device in Section VI using different UPC configurations to provide guidance on UPC parameter selection. Section VII discusses the experimental results. Finally, Section VIII concludes this article.

II. Proposed Ultimate Passivity Concept

This section establishes the necessary notations and introduces the novel concept of ultimate passivity within the context of a network denoted as N_M, comprising M subsystems as depicted in Fig. 1. This concept forms the foundational framework for the subsequent control synthesis of a pHRI system. This network configuration is referred to as an M-port network. The energy flowing into the network is in the positive direction, which is also unequivocally defined by the positive sign and the direction of the arrow in Fig. 1.

As pointed out in [13], the energy $E_i(t)$ of the ith subsystem is related to its force $f_i(t)$ and the velocity $v_i(t)$. More precisely, at the time instant t, the energy $E_i(t)$ can be computed as

$$E_i(t) = E_i(0) + \int_0^t f_i(\tau)v_i(\tau)d\tau, i = 1, \ldots, M. \quad (1)$$

With the prevalence of digital technology, both sensors and actuators are digital. That is, the sampled force inputs and velocity output signals are available, i.e., we can measure $\{v[j], f[j]\}_{j=1,2,\ldots}$. Here, for a continuous-time signal $s(t)$, its sampled signal is $s(t) = s[j] = s(jT_s), \forall t \in [jT_s, (j+1)T_s)$, where T_s is the sampling period.

If the sampling period is sufficient small (i.e., $T_s \to 0$), consequently, the energy $E_i(t)$ defined in (1) can be approximated by the following discrete-time version:

$$E_i(t) \approx E_i[k] = E_i(kT_s) = \sum_{j=0}^{k} f_i[j]v_i[j]T_s + E_i(0) \quad (2)$$

for all $t \in [kT_s, (k+1)T_s)$. By taking all M subsystems into consideration, the overall energy for the network N_M is

$$\begin{aligned} E(t) \approx E[k] &= \sum_{i=1}^{M} E_i[k] \\ &= \sum_{i=1}^{M}\sum_{j=0}^{k} f_i[j]v_i[j]T_s + \sum_{i=1}^{M} E_i(0) \end{aligned} \quad (3)$$

for all $t \in [kT_s, (k+1)T_s)$. This leads to the following definition of passivity for the discrete-time network [13].

Definition 1: An M-port network N_M with energy computed as (3) is passive if

$$E[k] \geq 0, \forall k \in \mathcal{N}_{\geq 0}. \quad (4)$$

We extend the notion of standard passivity by introducing an ultimately passive network. This novel concept allows for a relaxation of the passivity requirement at each time instant, as it places bounds on the energy exhibited while maintaining passivity in the steady-state condition.

Definition 2: A M-port network N_M with energy computed as (3) is ultimately passive if there exists a nonnegative pair (α_t, α_s) such that

$$\min_{k \in \mathcal{N}_{\geq 0}} E[k] \geq -\alpha_t, \quad (5)$$

$$\lim_{k \to \infty} E[k] \geq \alpha_s. \quad (6)$$

Remark 1: The ultimately passive network represents a more permissive form of a passive network, allowing for instances of nonpassive behavior characterized by $E[k] < 0$ for certain $k \in \mathbb{N}_{\geq 0}$, where $\mathbb{N}_{\geq 0}$ denotes the set of nonnegative integers. However, this concession is accompanied by the imposition of limits on the energy function's transient characteristics, which are bounded within the range defined by $-\alpha_t$ shown in (5). Furthermore, an ultimately passive system ensures passive behavior in steady-state, as described in (6). Notably, it is important to emphasize that the property of ultimately passive network is a broader one; a passive network N_M is inherently also ultimately passive, though the converse is not necessarily true.

Remark 2: While the constant pair (α_t, α_s) does not influence the ultimately passive characteristic, it does play a crucial role in shaping the transient dynamics of the M-port network system. This selection offers an additional avenue of design flexibility to engineering practitioners, allowing them to define

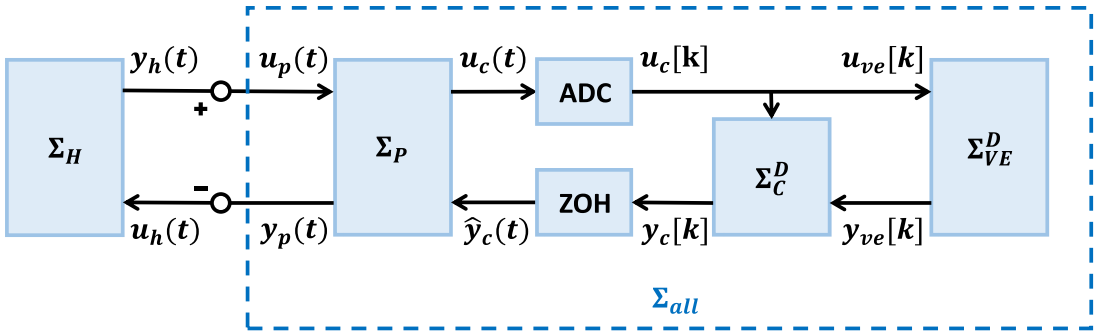

Fig. 2. Sampled-data pHRI system diagram (adapted from [13]).

the system's transient behaviors to align with their specific intentions and requirements. Experimental results (in Sections V and VI) present two examples of achieving the tradeoff between higher transparency and stability for an admittance interaction and between higher stiffness and stability for an impedance interaction.

Remark 3: It is well known that interconnected passive systems are passive, as established by [32, Theorem 6.3]. However, since ultimately passive network represents a less strict condition than standard passive network, it is important to recognise that the interconnection of ultimately passive systems does not automatically guarantee an ultimately passive overarching system. Consequently, a comprehensive analysis involving the integration of individual subsystems becomes indispensable to ensure that the overarching system is ultimately passive. Thereby, it introduces an elevated level of complexity to the design process of interconnected subsystems.

III. Problem Formulation

This section introduces the problem formulation of this work. It includes the components of the pHRI using input and output signals, followed by the needed assumptions for each component. In particular, two different types of controllers used for the VE are introduced with their characteristics. The control objective of this work is also presented.

A. Subsystems and Digital Implementation

The focus of this work is a class of sampled-data pHRI systems with its diagram shown in Fig. 2. It is noted that many nonlinear behaviors are included in the interaction. These nonlinear behaviors may result from the saturation of sensors and actuators of the robot, sampling behaviors of digital sensors and actuators, the quantisation of sensor data, and so on.

This work uses digital sensors and digital actuators operating at a sampling period T_s, which is assumed to be sufficiently small. For a continuous-time signal $s(t)$, after a sampler or ADC with the sampling period T_s, it becomes a discrete-time signal $s[k], \forall t \in [kT_s, (k+1)T_s), k \in \mathbb{N}_{\geq 0}$. For a discrete-time signal $s[k]$, after passing through a zero-order hold (ZOH), it becomes a piece-wisely continuous-time signal $\hat{s}(t) = \hat{s}(kT_s) = s[k], \forall t \in [kT_s, (k+1)T_s)$.

Such a sampled-data pHRI system consists of four subsystems: Σ_H represents the dynamics of the human, Σ_P is the dynamics of the plant (i.e., the robot), Σ_C^D is the digital low-level controller of the robot, and Σ_{VE}^D is the digital virtual environment. Each subsystem has its own input and output signals.

1) Human Dynamics Σ_H: The first subsystem Σ_H has its corresponding input u_h and output y_h. In pHRI, the input signal u_h is determined by the robot dynamics subsystem Σ_P (as such $u_h = y_p$), and the output signal y_h is directly applied to Σ_P (as such $y_h = u_p$). In an admittance-causality case, u_h denotes velocity and y_h denotes force, and vice versa for an impedance-causality case.

2) Robot Dynamics Σ_P: The input of Σ_P comes from two parts: one is denoted as u_p, which is related to the output of Σ_H (human subsystem) y_h. The other comes from y_c, which is the output of Σ_C^D (the robot low-level controller subsystem) for robot actuation. The output of the robot is y_p, which is applied to Σ_H via u_h.

3) Robot Low-Level Controller Σ_C^D: The digital low-level controller has the input of y_{ve}, which comes from the VE subsystem Σ_{VE}^D output and represents the desired VE rendering behavior to be implemented by Σ_C^D. When the low-level controller is responsible for dynamic compensation (i.e., gravity and/or friction), u_c is another input to Σ_C^D. The output of this controller subsystem is y_c, serving as the robot actuation signal.

4) Virtual Environment Σ_{VE}^D: The digital VE subsystem input u_{ve} upholds the relation of $u_{ve}[k] = u_c[k]$, and u_{ve} is related to the Σ_H output y_h given that the human interacts with the VE through the robot. The output of Σ_{VE}^D (denoted as y_{ve}) depicts the desired VE rendering behavior and acts as the input of Σ_C^D. The following approximated discrete-time second-order mass-damper-spring system (with a sampling period T_s) is employed in this study:

$$\Sigma_{VE}^D : \begin{cases} \begin{bmatrix} x_{ve,1}[k+1] \\ x_{ve,2}[k+1] \end{bmatrix} = \begin{bmatrix} 1 & T_s \\ -\frac{k_{ve}}{m_{ve}}T_s & 1-\frac{b_{ve}}{m_{ve}}T_s \end{bmatrix} \\ \qquad\qquad \begin{bmatrix} x_{ve,1}[k] \\ x_{ve,2}[k] \end{bmatrix} + \begin{bmatrix} 0 \\ \frac{1}{m_{ve}}T_s \end{bmatrix} u_{ve}[k], \\ y_{ve}[k] = \begin{bmatrix} 1 & 0 \end{bmatrix} \begin{bmatrix} x_{ve,1}[k] \\ x_{ve,2}[k] \end{bmatrix} \end{cases} \tag{7}$$

where the characteristics of Σ_{VE}^D are determined by the parameters of VE mass m_{ve}, VE damping coefficient b_{ve}, and VE spring constant k_{ve}.

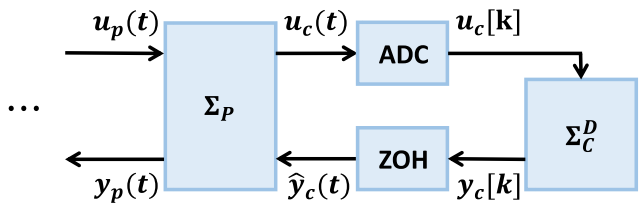

Fig. 3. System $\Sigma_{C,P}$ in the sampled-data pHRI system without VE.

With the consideration of sampling behaviors, this pHRI as shown in Fig. 2 has a continuous-time part and a discrete-time part. To simplify the analysis, we use the concept of discrete-time passivity to represent the sampled input–output relationship for each subsystem, which means such analysis relies on the digital implementation (i.e., sampled input and output signals) of the continuous-time part of the system. It is noted that by using the closeness of solution between the discrete-time trajectories and the sampled-data trajectories as shown in [33, Lemma 3], with sufficiently small sampling T_s, the concept of discrete-time passivity can be applied to conclude that this sampled-data system is passive.

B. Assumptions for pHRI

The interconnection of the systems Σ_C^D, ZOH and Σ_P is denoted as $\Sigma_{C,P}$ (see Fig. 3) and its energy is $E_{C,P}$. In this work, it is assumed that the robot low-level controller Σ_C^D cannot ensure the passivity of $\Sigma_{C,P}$. The following assumption is used to characterize such a behavior.

Assumption 1: For a given sampling period T_s, in the pHRI system without VE, the system $\Sigma_{C,P}$ satisfies

$$|E_{C,P}[k] - E_{C,P}[k-1]| \leq \gamma_{C,P}, \forall k = 1, 2, \ldots \tag{8}$$

where $E_{C,P}[k] = \sum_{j=0}^{k} u_p[j] y_p[j] T_s$, and $\gamma_{C,P}$ is a positive real constant. In an admittance-causality case, u_p is a force signal and y_p is a velocity signal, and vice versa for an impedance-causality case.

Remark 4: It is noted that in continuous-time, Assumption 1 indicates that there is no finite-escape phenomenon for the possibly nonlinear dynamics of $\Sigma_{C,P}$ (e.g. resulting from saturation or hysteresis of actuators), and such an assumption is always necessary for a general class of nonlinear dynamic systems [32, Chapter 3]. Assumption 1 also implies that the rate of energy change within $\Sigma_{C,P}$ is bounded, as such, this assumption holds true for all engineering systems because their energy cannot jump to positive infinity or negative infinity in one step. Different from the prevailing assumption in the existing literature, which requires both subsystems Σ_P and Σ_C^D to exhibit passivity, Assumption 1 is notably less restrictive. More importantly, given the presence of sampling and inherent nonlinear behaviors in pHRI, controllers designed in continuous-time may not consistently maintain their passivity [34], Assumption 1 is thus more feasible to satisfy in practical engineering applications. Furthermore, it accommodates a broader range of control laws to meet various performance criteria other than stability or passivity, such as tracking performance and robustness.

Similarly, instead of assuming Σ_H is passive, which is not always true as indicated in [35], the following assumption characterizes the subsystem Σ_H. To simplify the analysis, though Σ_H is defined in continuous time, its sampled input and output signals are used to characterize its passivity.

Assumption 2: In the pHRI system presented in Fig. 2, for a given sampling T_s, Σ_H satisfies

$$|E_H[k] - E_H[k-1]| \leq \gamma_H, \forall k = 1, 2, \ldots \tag{9}$$

where $E_H[k] = \sum_{j=0}^{k} u_h[j] y_h[j] T_s$, $u_h[k]$ and $y_h[k]$ are sampled signals of $u_h(t)$ and $y_h(t)$, respectively, and γ_H is a positive real constant.

C. Switching Between Two Control Laws

In this subsection, Σ_{all} represents the overall system presented in Fig. 2 with its energy denoted as E_{all}. In this system, we introduce two distinct control laws that operate within Σ_{PC}^D–representing the digital PC subsystem–as shown in Fig. 4. Each control law is tailored to a specific objective.

The first, referred to as the "conservative control design" and denoted as ${}^C\Sigma_{PC}^D$, aims to stabilize the depicted pHRI system in Fig. 4 under Assumptions 1–2. As this conservative controller is designed to stabilize the overall system, it is assumed that ${}^C\Sigma_{PC}^D$ satisfies the following assumption.

Assumption 3: For a given sampling T_s, a system Σ_C^D that satisfies Assumption 1 with $\gamma_{C,P}$ from (8), a system Σ_H that satisfies Assumption 2 with γ_H from (9), and a positive value κ, there exists a conservative PC ${}^C\Sigma_{PC}^D$ with parameters $\{m_{PC,C}, b_{PC,C}\}$. This controller ensures that the following inequality:

$$E_{all}[N + N_{all}] = \sum_{j=N}^{N+N_{all}} u_p[j] y_p[j] T_s \geq 0 \tag{10}$$

is satisfied for some finite $N_{all} \in \mathbb{N}_{\geq 0}$ if $E_{all}[N] \geq -\kappa$ for any $N \in \mathbb{N}_{\geq 0}$.

Remark 5: This assumption posits the existence of a conservative configuration $b_{PC}[k] = b_{PC,C}$ and $m_{PC}[k] = m_{PC,C}$, which is capable of stabilizing a nonpassive system with bounded energy $E_{all}[N] \geq -\kappa$ by taking the system back to the passive state (so guaranteeing stability). This assumption also specifies that if the conservative controller has been switched ON, within the next N_{all} steps, the overall energy satisfies $E_{all}[N + N_{all}] \geq 0$. It is noted that Assumption 3 is related to Assumptions 1 and 2, as the bounded energy changes in subsystems ensure the energy of the overall system is bounded, allowing the conservative controller to be able to ensure that the condition (10) holds. In the combination of $\{m_{PC,C}, b_{PC,C}\}$, $b_{PC,C}$ is necessary for excess energy dissipation, and $m_{PC,C}$ is an option to be used to assist system stabilisation (usually for admittance-causality) without introducing too much complexity in parameter tuning for such a configuration.

In contrast, the second control law, denoted as ${}^N\Sigma_{PC}^D$ with parameters $\{m_{PC,N}, b_{PC,N}\}$, is crafted to achieve a desired VE behavior of nominal performance. This VE can correspond to an ideal behavior for the haptic system to achieve, with

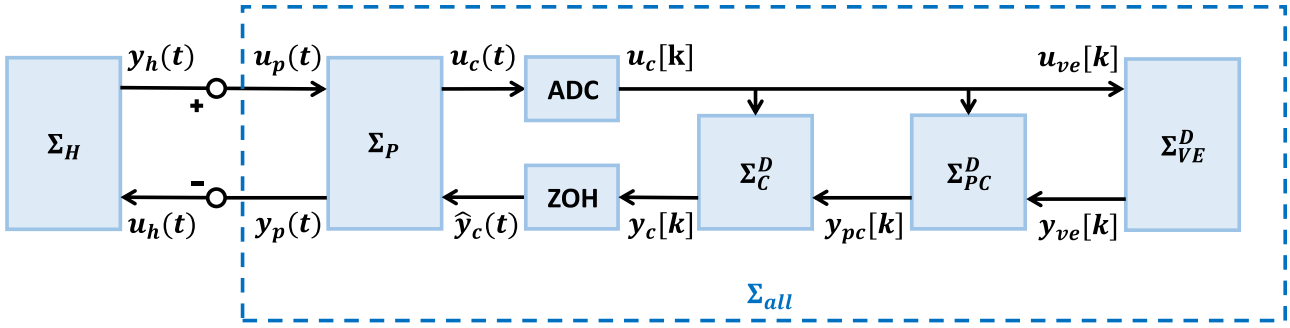

Fig. 4. Sampled-data pHRI system with a digital Passivity Controller subsystem denoted as Σ_{PC}^D (adapted from [13]). The output of Σ_{PC}^D is y_{pc}, which is a resultant signal combining both the desired VE rendering behavior (depicted by y_{ve}) and the PC action, to be implemented by the robot low-level controller.

${}^N\Sigma_{PC}^D$ effectively acting as a bypass for the system to best render the VE. If a nominal performance that deviates from the pre-defined VE is desired, it is also possible to setup ${}^N\Sigma_{PC}^D$ parameters to be nonnull (i.e., not bypassing the system), and the proposed algorithm can still function effectively. It is important to emphasize that this second control law does not guarantee the passivity or stability of the overall pHRI system shown in Fig. 4. It is also highlighted that as indicated in [36], [37], transparency or stiffness and stability are two contradicting requirements.

It is assumed that there are two control laws designed for VE for different purposes: One is the conservative control law ${}^C\Sigma_{PC}^D\ \{m_{PC,C}, b_{PC,C}\}$ satisfying Assumption 3 and the other is the nominal controller ${}^N\Sigma_{PC}^D\ \{m_{PC,N}, b_{PC,N}\}$ to achieve the nominal performance. The control objective of this work is to design an appropriate observer to estimate the energy flow for Σ_{PC}^D. Furthermore, the projected energy values will serve as the foundation for crafting a suitable control algorithm, which we have labelled as "passivity control". This algorithm is designed to attain the targeted nominal performance while ensuring some stability properties through the lens of ultimate passivity. More precisely, we are hoping to achieve the following.

1) The overall system Σ_{all} is ultimately passive by using an appropriate PC.
2) The nominal performance is kept as long as possible by tuning the parameters of the passivity controller.

IV. Ultimate Passivity Implementation Framework

This section proposes a UPC to ensure that the overall system Σ_{all} is ultimately passive when both the nominal controller ${}^N\Sigma_{PC}^D$ and the conservative controller ${}^C\Sigma_{PC}^D$ exist. Such a UPC is based on the estimated energy from the passivity observer. The role of UPC is to balance stability and nominal performance. Within this section, we employ an abstract nominal performance for the purpose of analysis. The experimental implementation examples are then provided in Sections V and VI.

A. Proposed Framework

The diagram of the proposed framework is shown in Fig. 5. The logic of the design is quite simple: if ${}^N\Sigma_{PC}^D$ is not able to make Σ_{all} ultimately passive, the conservative controller ${}^C\Sigma_{PC}^D$ will be switched on to ensure the ultimate passivity. If the system

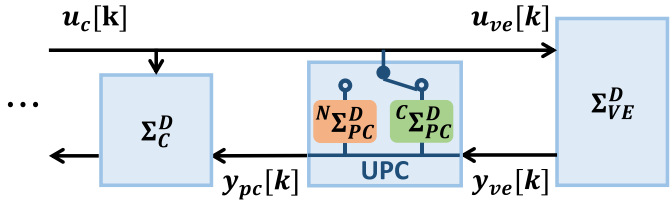

Fig. 5. Proposed Ultimately Passive Controller (UPC) framework for the sampled-data pHRI system.

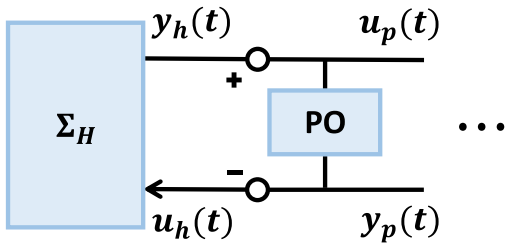

Fig. 6. Passivity Observer (PO) for the sampled-data pHRI system.

is already ultimate passive using the conservative controller, the ${}^N\Sigma_{PC}^D$ will be switched ON to ensure the nominal performance.

In this figure, the UPC is a simple switch, which is critical to ensure the balance between nominal performance and passivity. Under such a situation, the focus of UPC will be on the design of switching laws. The challenge is to decide when to switch back to the nominal controller ${}^N\Sigma_{PC}^D$ and provide sufficient conditions to ensure Σ_{all} is ultimately passive. The design requirements are as follows.

1) There are finite times of switching within a finite time interval (i.e. user-defined interval of interest during pHRI activities).
2) In order to ensure the inequality (6) holds, the conservative model ${}^C\Sigma_{PC}^D$ needs to be switched ON with no further switching when $t \to \infty$.

As shown in Fig. 6, the role of the PO is to try to estimate the energy flow of Σ_{all}.

B. Passivity Observer

In this subsection, we would like to estimate the energy flow of Σ_{all}, which serves as the criterion for the design of UPC. Here,

Σ_{all} denotes the overall system, its energy can be calculated as

$$E_{all}[k] = \sum_{n=0}^{k} u_p[n] y_p[n] T_s + E_{all}[0] \tag{11}$$

where $u_p[n]$ is the sampled input of the robot Σ_P and $y_p[n]$ is the sampled output of Σ_P. We also use an estimation of the future energy (one-step prediction)

$$\begin{aligned} \hat{E}_{all}[k+1|k] &= E_{all}[k] + u_p[k+1] y_p[k+1] T_s \\ &\approx E_{all}[k] + u_p[k] y_{ve}[k] T_s \end{aligned} \tag{12}$$

when T_s is sufficiently small relative to the change of the Σ_{all}. Here, $\hat{E}_{all}[k+1|k]$ indicates the predicted value based on the measurements from $E_{all}[k]$ and the VE command $y_{ve}[k]$ to be applied in the future step [14].

C. Ultimately Passive Controller (UPC)

The proposed UPC is designed on the basis of the predicted energy. It generates the necessary switching between the nominal controller ${}^{N}\Sigma^{D}_{PC}$ and the conservative controller ${}^{C}\Sigma^{D}_{PC}$ independently of the VE by selecting an upper bound $\bar{E} > 0$ and a lower bound $-\underline{E} < 0$.

A logic variable is introduced at each sampling instant k

$$L_s[k+1] = \begin{cases} -1 & \text{if } \hat{E}_{all}[k|k-1] \geq -\underline{E} \\ & \quad \wedge \hat{E}_{all}[k+1|k] < -\underline{E} \\ 1 & \text{if } \hat{E}_{all}[k|k-1] \leq \bar{E} \\ & \quad \wedge \hat{E}_{all}[k+1|k] > \bar{E} \\ 0 & \text{else} \end{cases} \tag{13}$$

where $\hat{E}_{all}[k+1|k]$ is defined in (12). Here the notion of $\wedge$ indicates that two conditions have to be satisfied simultaneously.

We also count the number of switches using a counter

$$N_c[k+1] = \begin{cases} N_c[k] & \text{if } L_s[k+1] = 0 \\ N_c[k] + 1 & \text{if } L_s[k+1] \neq 0 \end{cases} \tag{14}$$

where $N_c[0] = 0$. This leads to the following UPC:

$$\Sigma^{D}_{PC}[k+1] = \begin{cases} {}^{N}\Sigma^{D}_{PC}[k+1] & \text{if } L_s[k+1] = 1 \wedge N_c[k] \leq N_f \\ {}^{C}\Sigma^{D}_{PC}[k+1] & \text{if } L_s[k+1] = -1 \\ \Sigma^{D}_{PC}[k] & \text{else} \end{cases} \tag{15}$$

where N_f is an integer representing maximum allowable switches.

Remark 6: When the maximum allowable switches N_f is reached and the conservative controller ${}^{C}\Sigma^{D}_{PC}$ is switched on, the energy of the overall system E_{all} may accumulate until the end of the user-defined operation interval of pHRI. In practice, engineers commonly introduce an additional parameter for energy ceiling to cap E_{all}, as described in [15], which discards potentially dangerous excessive accumulated energy. This energy accumulation can also be more systematically managed by the method in [17] to avoid the "memory effect."

D. Main Result

In this subsection, the following theorem shows that the proposed algorithm can ensure that the pHRI system with Assumptions 1, 2, and 3 is ultimately passive. These three assumptions are necessary. The first two prevent scenarios where the energy of unstable subsystems drops to negative infinity within a single step, leading to the proposed UPC being ineffective. With Assumptions 1 and 2 held, the third assumption ensures the existence of a conservative controller, which can increase the energy of Σ_{all} to positive so that the stability is guaranteed.

Theorem 1: Assume that Assumptions 1, 2, and 3 hold for the pHRI system presented in Fig. 4. For any given $E_{all}[0] = E_0$, there is a positive pair $\{\bar{E}, \underline{E}\}$ and a positive integer N_f such that the proposed algorithm, which consists of the energy observer (11), the predicted energy (12), the logic (13), the counter (14), and UPC (15), ensures the pHRI system ultimately passive.

Proof: In the proof, we consider the worst-case scenario where $E_{all}[0] = E_0 < 0$. A similar argument applies when $E_{all}[0] = E_0 \geq 0$. It is noted that by selecting $\underline{E}$ such that the following inequality holds:

$$E_0 \geq -\underline{E}$$

the proposed UPC (15) always has a lower bound $-\underline{E}$ and an upper bound $\bar{E}$ provided that Assumptions 1, 2, and 3 hold.

For a given N_f, there exists a time instant T_f such that after $k \geq T_f$, the conservative controller will switch on. Along with Assumption 3, it can ensure that the overall system is passive at a steady state. This concludes that the overall pHRI system is ultimately passive. □

Remark 7: When the pHRI system operates within a defined finite interval $[0, T]$, the occurrences of switching in this sampled-data system remain finite for any given fixed sampling period T_s, since T_s cannot approach zero due to practical constraints. Also, appropriately configured UPC should prevent it from extremely frequent switching. Consequently, selecting N_f is not always needed. However, switching introduces discontinuity, potentially leading to more oscillations. Engineering practitioners thus can determine a maximum allowable switching N_f for a selected time interval $[0, T]$ as a design choice based on application needs to prevent excessive switching, which ensures optimal performance and stability even in the most unstable scenarios of interaction.

The proposed UPC, which encompasses the switching mechanism (15), along with the energy observer (11), the predictive energy estimation (12), the governing logic (13), and the counter mechanism (14), offers a comprehensive and coherent approach to optimize the performance equilibrium between two distinct controllers: The conservative variant ${}^{C}\Sigma^{D}_{PC}$ and the nominal counterpart ${}^{N}\Sigma^{D}_{PC}$. This optimization is achieved through the configuration of the parameters $\{\bar{E}, \underline{E}, N_f\}$.

In essence, a narrower gap between $\bar{E}$ and $-\underline{E}$ implies that the action time of conservative controller ${}^{C}\Sigma^{D}_{PC}$ is relatively short when it is activated each time, corresponding to a shorter period of nominal performance sacrifice on every occasion. However, this design choice could lead to more frequent switches–so more frequent performance sacrifice–throughout the operation,

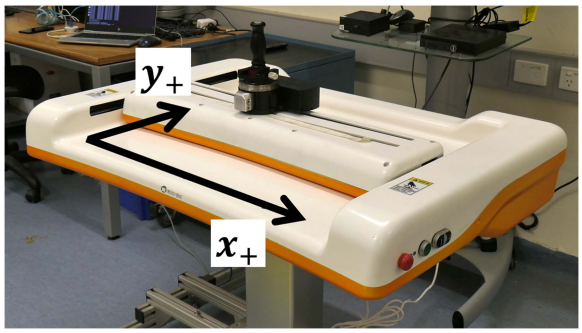

Fig. 7. 2-D admittance device used in the experiment.

reflecting a discernible design tradeoff. The selection of these parameters is inherently dependent on the specific application context, but the effect of different parameters and a general guide for their selection is presented in the experimental results (in Section VI-C).

V. Admittance Causality Experiment

To evaluate the proposed UPC, experiments were first conducted on an admittance-based system. The system comprises a human operator (Σ_H), a robot (Σ_P), a robot low-level controller (Σ_C), a passivity observer, a passivity controller (Σ_{PC}), and a virtual environment (Σ_{VE}) as shown in Fig. 4.

A. Experiment Setup and Design

An ArmMotus-M2 (Fourier Intelligence, Shanghai, China), shown in Fig. 7, was used as the admittance-based device for this experiment. It is a 2-D planar system with a workspace of $575 \times 400\,\text{mm}$ and equipped with a handle mounted on two strain gauges. The passivity control algorithms were implemented in C++ using the CORC framework [38] with a control loop running at 1 kHz, performing the kinematic and interaction force acquisition at the same frequency. This sufficiently small sampling period ensured the feasibility of using the discrete-time version of passivity defined in Equations (3) and (4). The position and force resolutions were $0.003\,\text{mm}$ and $0.06\,\text{N}$, respectively.

It is noted that for an admittance device, it is challenging to render high transparency (i.e., a low virtual mass and low virtual damper) when the human operator (HO) suddenly exhibits a high impedance [6]. Therefore, a highly transparent VE was rendered in the x-direction with an admittance of $\{m_{ve} = 0.24\,\text{kg}, b_{ve} = 0.08\,\text{Ns}\cdot\text{m}^{-1}\}$ to evaluate the effectiveness of UPC in haptic interaction.

In order to evaluate the overall system performance in rendering the more "transparent" possible behavior, an effective virtual mass m_e was defined as the overall mass value to be rendered in the system, and a resulting effective virtual damping b_e was calculated as

$$b_e = \frac{f_m T_s - m_e v_d + m_e \dot{x}_m}{v_d T_s} \tag{16}$$

where f_m is the measured interaction force in the x-direction, v_d is the desired velocity in the x-direction to be implemented by the low-level controller, $\dot{x}_m$ is the measured velocity of the robot end-effector in the x-direction, m_e is the effective virtual mass value, and T_s is the system control loop period. A smaller m_e and b_e value indicate a more transparent system where the overall rendered behavior is closer to the intended VE.

During the experiment, the HO held the robot end-effector while exhibiting high stiffness to the device (i.e., with muscles co-contracted). Two different scenarios were tested for the admittance causality experiment: HO's single high stiffness behavior and repeated high stiffness behaviors.

B. HO's Single High Stiffness Behavior

In this task, the HO held the robot end-effector and performed a sudden movement followed by a sudden stop with persistent high arm stiffness (i.e. maximum arm co-contraction). The proposed UPC was compared to ①the PC proposed by [14] (referred to as "classic PC"), and ②the energy tank approach proposed by [25] (referred to as "tank") which were implemented on the device.

The UPC switched between the nominal controller with parameters $\{m_{PC,N} = 0, b_{PC,N} = 0\}$ (bypassing the system) and the conservative controller with parameters $\{m_{PC,C} = 0.1\,\text{kg}, b_{PC,C} = 50\,\text{Ns}\cdot\text{m}^{-1}\}$. The UPC's upper and lower bound of energy were tuned to be $\bar{E} = 0.1\,\text{J}$ and $-\underline{E} = -0.1\,\text{J}$ respectively. For the tank implementation [25], the following parameters were used: Oscillation detection threshold $\epsilon = 3.7\,\text{m}\cdot\text{s}^{-2}$ (defined according to the calibration procedure in [25]); forgetting factor $\beta = 0.1$; upper bound of inertia variation $\Delta M = 0.5\,\text{kg}$; tank storage upper bound $\bar{T} = 0.2\,\text{J}$, and lower bound $\delta = 0.05\,\text{J}$.

Results for the different approaches are presented in Fig. 8. As expected, as a consequence of HO's sudden movement, stop, and persistent arm stiffness, combined with a low virtual mass of VE, the robot end-effector kept oscillating when the PC was OFF [Fig. 8(a)]. At the same time, the PO-estimated energy fell to negative and remained dropping.

Fig. 8(b) shows the impossibility of the classic PC approach to stabilize the system in the same conditions. This is due to a delay of approximately 6 ms in this device's velocity control loop (from when a velocity command was generated to when the corresponding velocity was measured). This delay leads the PC-produced velocity to be out of phase with the interaction force. This phase lag makes the system especially inappropriate for using the classic PO-PC approach, as this strategy relies on an online calculation of the PC virtual damping which is directly affected by the asynchronicity of the velocity and force signals, leading to continuing large oscillations, only bounded by the force acquisition saturation (at $100N$) and velocity command saturation (for safety reasons) at $1.8\,\text{m}\cdot\text{s}^{-1}$ (just below the system hard cutoff at $2.0\,\text{m}\cdot\text{s}^{-1}$).

For the same scenario, the tank approach stabilized the system when the HO exhibited high stiffness. At the time that the measured acceleration tracking error exceeded the predefined oscillation detection threshold ϵ, incremental virtual mass and damping were implemented in the system [see Fig. 8(c)], representing a transparency sacrifice.

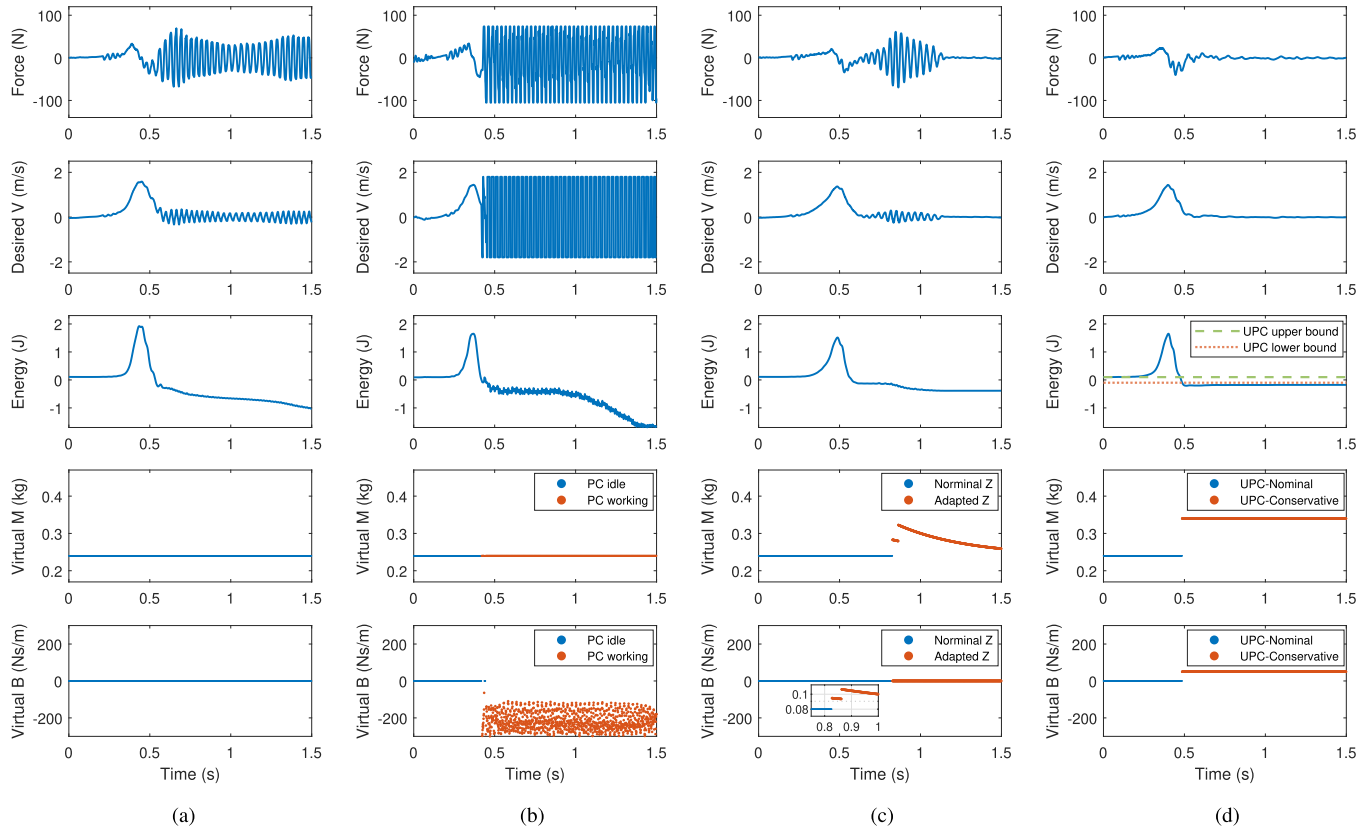

Fig. 8. System performance of the admittance device when the HO held the device end-effector and performed a sudden movement (i.e., first rapid increase of force) followed by a sudden stop (i.e., first rapid descent of force) with persistent high stiffness, under the conditions of (a) PC switched OFF, (b) the classic PC [14], (c) the tank [25], and (d) the proposed UPC. The inserted graph in (c) zooms in to show the detailed changes of effective virtual damping for the tank. The PO-estimated energy (third row) was not used for the tank implementation but provided for comparison. (a) Without PC. (b) Classic PC. (c) Tank. (d) UPC.

The UPC also stabilized the system promptly as shown in Fig. 8(d). The UPC switched to the conservative controller when its lower bound of energy ($-\underline{E} = -0.1\,\mathrm{J}$) was reached, resulting in higher effective virtual mass and damping values $\{m_e = 0.34\,\mathrm{kg}, b_e = 50.08\,\mathrm{Ns}\cdot\mathrm{m}^{-1}\}$ so lower transparency. It is noted that in this task, the HO maintained their high stiffness behavior (i.e., arm co-contraction) to the end of the trial, so the robot end-effector remained (almost) stationary. This led to a very slow dissipation of excess energy–as the dissipation relies on movement–and the UPC thus remained in the conservative mode (before reaching the upper bound of energy $\bar{E}$).

C. HO's Repeated High Stiffness Behavior

For the second task, the HO moved the robot end-effector in the x-direction gently most of the time, but for three short episodes of high stiffness behavior (i.e., arm co-contractions) followed by one longer episode of high stiffness behavior. The shorter arm co-contractions lasted for less than 1 s, and the longer one was kept for approximately 2 s. Given the capability of the tank [25] and UPC in stabilizing the system shown in Section V-B, these two approaches were subsequently evaluated in this scenario.

Here the UPC switched between the nominal controller $\{m_{PC,N} = 0, b_{PC,N} = 0\}$ and the conservative controller $\{m_{PC,C} = 0.1\,\mathrm{kg}, b_{PC,C} = 50\,\mathrm{Ns}\cdot\mathrm{m}^{-1}\}$, determined by the upper bound ($\bar{E} = 0.1\,\mathrm{J}$) and the lower bound ($-\underline{E} = -2\,\mathrm{J}$) of energy. A lower $-\underline{E}$ less than 0 was selected for this task, to demonstrate how nonpassive transient behavior can be allowed in order to produce less frequent but longer PC corrections. It is expected to sacrifice the rendering performance less frequently while still ensuring the system to be ultimately passive. The tank implementation used the same parameters provided in Section V-B.

Not surprisingly, as shown in Fig. 9, both the tank and the UPC stabilized the system during the longer high stiffness episode (corresponding to the fourth rapid ascent of force in the figure). However, the tank and the UPC exhibited distinct performance in terms of the effective virtual mass m_e and damping b_e throughout the trial. The tank increased m_e and b_e four times in response to HO's first three shorter high stiffness behavior and the fourth longer one [Fig. 9(a)]. Each episode led to an occurrence of transparency loss.

In contrast, the UPC maintained the system at its intended transparency most of the time even during the three short high stiffness episodes [corresponding to the first three rapid ascents of force in Fig. 9(b)]. It only altered m_e and b_e once at the HO's fourth high stiffness behavior (the longer maximum arm co-contraction) when the energy level effectively dropped bellow the UPC's lower bound of energy ($-\underline{E} = -2\,\mathrm{J}$). After that, the UPC kept applying the conservative controller–resulting in sacrificed performance $m_e = 0.34\,\mathrm{kg}$ and $b_e = 50.08\,\mathrm{Ns}\cdot\mathrm{m}^{-1}$–to

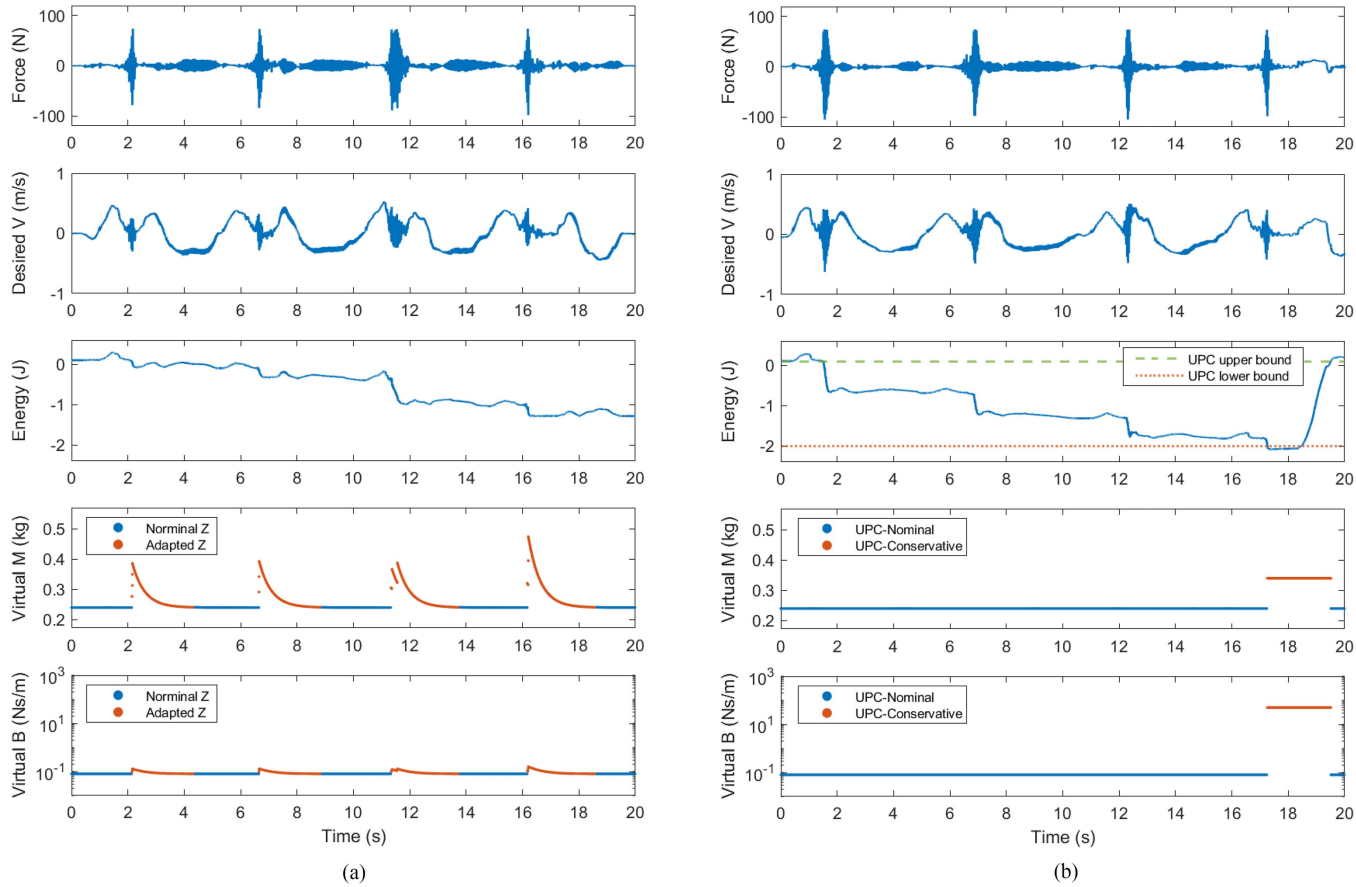

Fig. 9. System performance of the admittance device when the HO moved the robot end-effector gently most of the time and performed three short episodes followed by a longer episode of high stiffness (i.e., visible as the four higher force episodes in the top row) with (a) the tank approach [25], and (b) the proposed UPC. The PO-estimated energy (third row) was not used for the tank implementation but is provided for comparison. (a) Tank. (b) UPC.

dissipate excess energy until the PO-estimated energy reached the energy upper bound ($\bar{E} = 0.1\,\mathrm{J}$) to regain passivity. The UPC then switched back to the nominal controller, and the system restored its intended transparency $\{m_e = 0.24\,\mathrm{kg}, b_e = 0.08\,\mathrm{Ns}\cdot\mathrm{m}^{-1}\}$.

VI. Impedance Causality Experiment

The proposed UPC was then evaluated on an impedance-based system. The first experiment (single-contact scenario in Section VI-B) aims to evaluate the generalizability of the UPC approach to impedance causality and its comparison with the classic PC approach, whereas a second experiment (repeated-contact scenario in Section VI-C) specifically aims to illustrate the effect of different UPC parameters and serve as a general guide for their selection.

A. Experiment Setup and Design

Algorithms were implemented on a 3-D impedance device (see Fig. 10). The device workspace can be approximated by a cube with dimensions $450 \times 700 \times 400\,\mathrm{mm}$, and it was always operated in a gravity-compensated and friction-compensated mode during the experiment. The passivity control algorithms were implemented in C++ using the CORC framework [38] with a control loop running at 1 kHz. The position and force resolutions were 0.05 mm and 0.09 N, respectively.

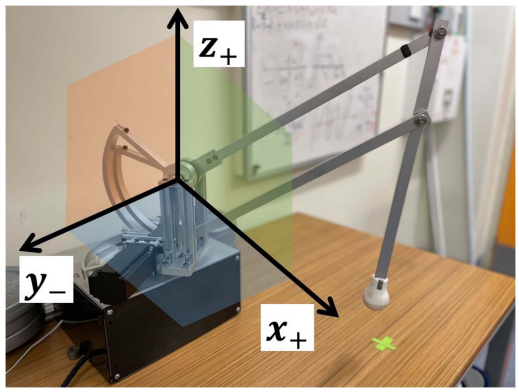

Fig. 10. 3-D impedance device used in the experiment.

In contrast to admittance causality, the challenge for an impedance device is to render high stiffness when the HO exhibits a low impedance. To evaluate the efficacy of UPC in such a challenging circumstance, a commonly used simplified case of haptic rendering was modelled, which relied on the simplified modelling of penetration depth as a virtual spring [30]. Specifically, a high stiffness VE ("virtual wall") was built below

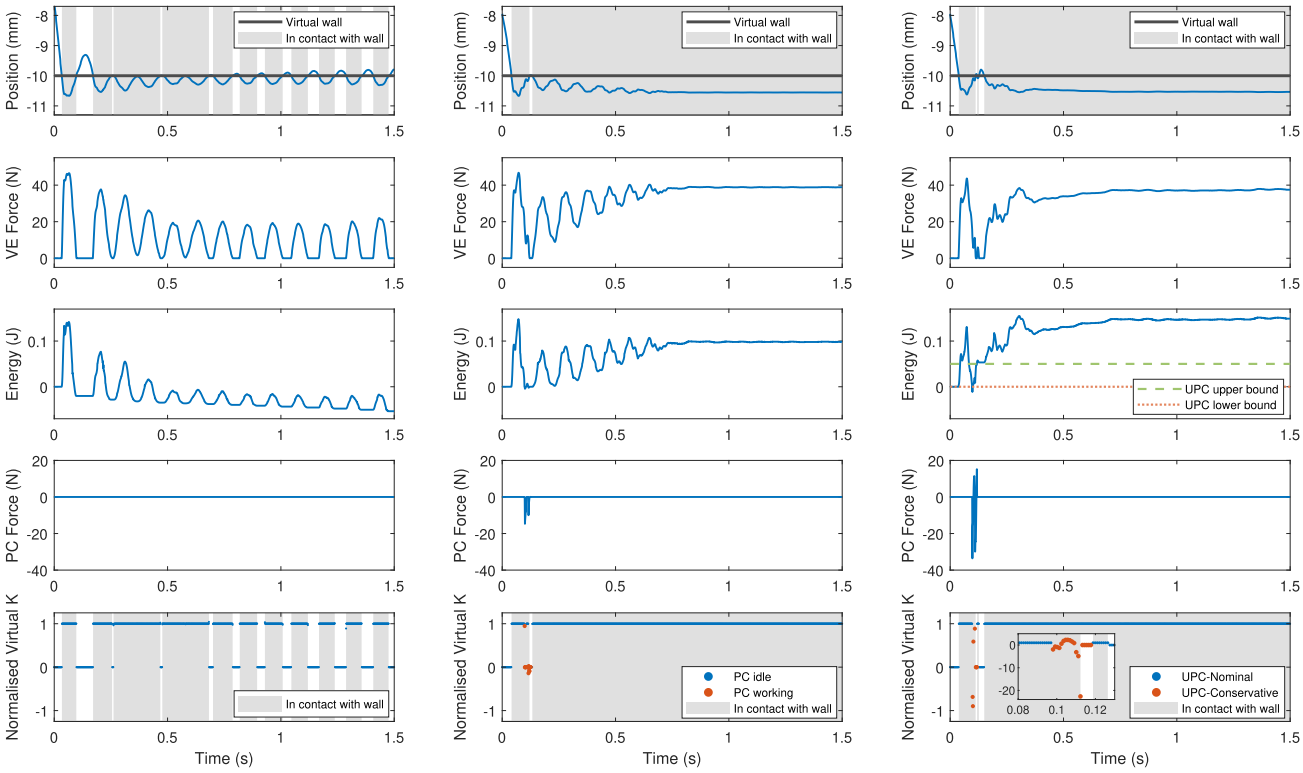

Fig. 11. System performance of the impedance device when the HO held the device end-effector and performed a single contact with the virtual wall, under the conditions of (a) PC switched OFF, (b) the classic PC proposed by [14], and (c) the proposed UPC. The inserted graph in (c) shows the normalized effective virtual stiffness values outside the y-axis limit. (a) Without PC. (b) Classic PC. (c) UPC.

a horizontal plane of $z_0 = -10\,\text{mm}$ with a spring-type stiffness of $k_{ve} = 7\,\text{kN}\cdot\text{m}^{-1}$.

To evaluate the overall rendered performance, a resulting effective virtual stiffness k_e for each contact was computed as

$$k_e = \begin{cases} \frac{f_d}{z_0 - z_m} & \text{if } z_m < z_0 \\ 0 & \text{if } z_m \geq z_0 \end{cases} \tag{17}$$

where f_d is the desired force to be applied by the robot in the z-direction, z_m is the measured position of the robot end-effector in the z-direction, and $z_0 = -10\,\text{mm}$ is the position of the virtual wall. Then, the normalized effective virtual stiffness $k_{e.nom}$ was obtained by

$$k_{e.nom} = \frac{k_e}{k_{ve}} \tag{18}$$

where k_e is the effective virtual stiffness calculated from (17), and k_{ve} is the desired stiffness of VE which is $7\,\text{kN}\cdot\text{m}^{-1}$ in this case. When the robot end-effector is in contact with the virtual wall, $k_{e.nom} < 1$ indicates that the overall rendered stiffness is inferior to its desired stiffness (i.e., a loss of performance).

During the experiment, the HO held the device end-effector to approach and contact the virtual wall. Two distinct interaction scenarios were tested for the impedance causality experiment: single contact and repeated contacts.

B. *Single Contact With Virtual Wall*

In this scenario, the operator held the device end-effector to approach the virtual wall and did not attempt further contact with the virtual wall after the first bounce. For comparison, the classic PC algorithm [14] and the proposed UPC were evaluated.

The UPC was setup to switch between the nominal controller with parameters $\{m_{PC,N} = 0, b_{PC,N} = 0\}$, acting as a bypass for the system, and the conservative controller with parameters $\{m_{PC,C} = 0, b_{PC,C} = 60\,\text{Ns}\cdot\text{m}^{-1}\}$. The UPC was tuned with an upper bound of energy $\bar{E} = 0.05\,\text{J}$, and a lower bound of energy $-\underline{E} = 0\,\text{J}$, set to exhibit a behavior similar to the classic PC for comparison.

When the PC was turned OFF, the end-effector kept bouncing in the z-direction once it bumped into the virtual wall [see Fig. 11(a)]. The PO-estimated energy was observed to drop below zero, which reflected the unstable behavior caused by the stiff VE.

In the same conditions, the classic PC dissipated just enough excess energy when the system shifted to nonpassive, resulting in constantly positive PO-estimated energy [see Fig. 11(b)]. As expected, it is noted that $k_{e.nom}$ dropped below its desired value when the classic PC was triggered (justified by the nonzero PC force), indicating that the PC virtual damper effectively reduced the overall rendered stiffness.

Similarly, the UPC was able to stabilize the system in a timely manner and maintain the system passive as shown in

Fig. 11(c). The UPC started dissipating excess energy from the PO-estimated energy turning negative (i.e., below $-\underline{E} = 0\,\text{J}$) until reaching the predefined UPC upper bound of energy ($\bar{E} = 0.05\,\text{J}$ in this case). In this procedure, the normalized effective virtual stiffness was observed to drop significantly to $k_{e.nom} = -22.63$, showing a sharper and harsher reaction than the classic PC.

C. Repeated Contacts With Virtual Wall

In this second scenario, the HO held the device end-effector to approach the virtual wall and kept trying to maintain contact with the wall during 5 s. This scenario is more representative of what a haptic exploration would be where the operator is almost continuously in contact with a virtual stiff shape. In addition to the previous experiment, several different values of UPC's lower bound of energy $-\underline{E}$ and virtual damping $b_{PC,C}$ were implemented to provide a general indication of UPC parameter selection.

1) Comparison Between Classic PC and UPC: In this trial, the UPC switched between the nominal controller $\{m_{PC,N} = 0, b_{PC,N} = 0\}$ and the conservative controller $\{m_{PC,N} = 0, b_{PC,C} = 60\,\text{Ns}\cdot\text{m}^{-1}\}$, determined by the upper bound ($\bar{E} = 0.05\,\text{J}$) and the lower bound ($-\underline{E} = 0\,\text{J}$) of energy. When the HO bumped into the virtual wall in a repeated manner with the classic PC turned ON, the system retained positive energy (passive state). However, its $k_{e.nom}$ fell down below its desired value almost at each contact as shown in Fig. 12(a). In contrast, Fig. 12(b) shows that the UPC maintained the system at its desired stiffness level most of the time and was only altered four times (approximately at 1.3 s, 2.5 s, 3.6 s, and 4.8 s).

2) Effect of Lower Bound of Energy ($-\underline{E}$): When the same virtual damping ($b_{PC,C} = 60\,\text{Ns}\cdot\text{m}^{-1}$) and upper bound of energy ($\bar{E} = 0.05\,\text{J}$) were used, all the UPCs with various lower bound of energy values ($-\underline{E} = 0, -0.05, -0.1\,\text{J}$) were able to restore the passivity of the system. However, the UPC with $-\underline{E} = 0\,\text{J}$ switched to the conservative controller four times (representing a stiffness sacrifice), while this switching happened only twice for the UPC with $-\underline{E} = -0.05\,\text{J}$ and once for the UPC with $-\underline{E} = -0.1\,\text{J}$ in the five-second interval and for the same number of contacts with the virtual wall [see Fig. 12(b), (c), and (d)]. This illustrates that a lower value of $-\underline{E}$ allows more frequent nonpassive transients, such that the rendering performance can be sacrificed less frequently while keeping the system ultimately passive.

3) Effect of Conservative Controller Damper ($b_{PC,C}$): Similarly, when the same upper bound ($\bar{E} = 0.05\,\text{J}$) and lower bound of energy ($-\underline{E} = -0.1\,\text{J}$) were used, all the UPCs with various virtual damping values ($b_{PC,C} = 20, 60, 100\,\text{Ns}\cdot\text{m}^{-1}$) brought the system back to positive energy (passive state). More importantly, with an increasing $b_{PC,C}$, the conservative controller action time (i.e., dissipating excess energy from $-\underline{E}$ triggered until $\bar{E}$ reached) reduced from 0.29 to 0.10 s and 0.02 s, respectively [see Fig. 13(a), (b), and (c)]. At the same time, the absolute value of peak PC force–as a result of the implementation of UPC virtual damping–increased from 12.9 to 52.5 N and 83.9 N, respectively [see Fig. 13(a), (b), and(c)]. This shows how selecting a larger UPC virtual damping leads to a shorter but heavier performance sacrifice. This sacrifice was clearly visible on the drop of the effective virtual stiffness, with a minimum value $k_{e.nom} = -15.5$ for a $b_{PC,C}$ of $100\,\text{Ns}\cdot\text{m}^{-1}$ compared to only $k_{e.nom} = -3.2$ for a $b_{PC,C}$ of $20\,\text{Ns}\cdot\text{m}^{-1}$.

VII. Discussion

A. Performance Comparison

The proposed UPC aims to allow for a less frequent sacrifice of performance while still ultimately maintaining the system passive and so safe for the user. Experiments conducted on both admittance and impedance devices show that the UPC is able to stabilize pHRI systems and can maintain an overall better performance (i.e., render intended VE) most of the time compared to classic PC and tank approaches.

Specifically, the UPC first showed the ability of maintaining the pHRI system stable when the HO performed single destabilizing behaviors. For example, in the implementation on the admittance-causality system (Section V-B), where rendering a very low impedance is challenging when the HO displays a high stiffness, the tank approach [25] stabilized the system during the HO's single persistent high stiffness behavior. In comparison, the UPC stabilized the system even more promptly in this scenario, as it did not wait to be activated until the robot end-effector oscillations intensified to a predefined oscillation detection threshold like the tank approach. Similarly, the implementation on the impedance-causality system (Section VI-B), where rendering a high-stiffness VE is challenging, showed that the classic PC was able to stabilize the bouncing robot end-effector in the scenario with a single contact with the virtual wall, as previously shown in [14]. In this scenario, due to a larger response, the UPC provided a faster stabilization, effectively reducing the number of bounces, but at the cost of a larger drop of performance.

It is in the HO's repeated destabilizing behaviors, more representative of actual pHRI use-cases, that the UPC differed more significantly from the tank and the classic PC approaches. In the admittance-causality experiment (Section V-C), the UPC more heavily sacrificed performance only once and maintained the intended VE transparency at all other times during the HO's repeated high stiffness episodes. Such a strategy effectively reduced the frequency of performance sacrifice compared to the tank approach, where the intended transparency was affected at each HO's high stiffness episode, even if such episodes were short. Such approach could thus handle scenarios, reported by Meulman et al. [39], where a lower-limb exoskeleton contacts with the ground during the stance phase, highly increasing the environment stiffness and thus problematic for admittance devices. While in their approach the system admittance can be tuned based on the exoskeleton phase (stance detection), it might be desirable to automate such switching as it could be done with a UPC implementation.

Likewise, in the repeated-contact scenario of the impedance-causality experiment (referred to Section VI-C), the classic PC was activated at almost each contact as expected, effectively rendering a stiffness lower than intended for the user. Instead,

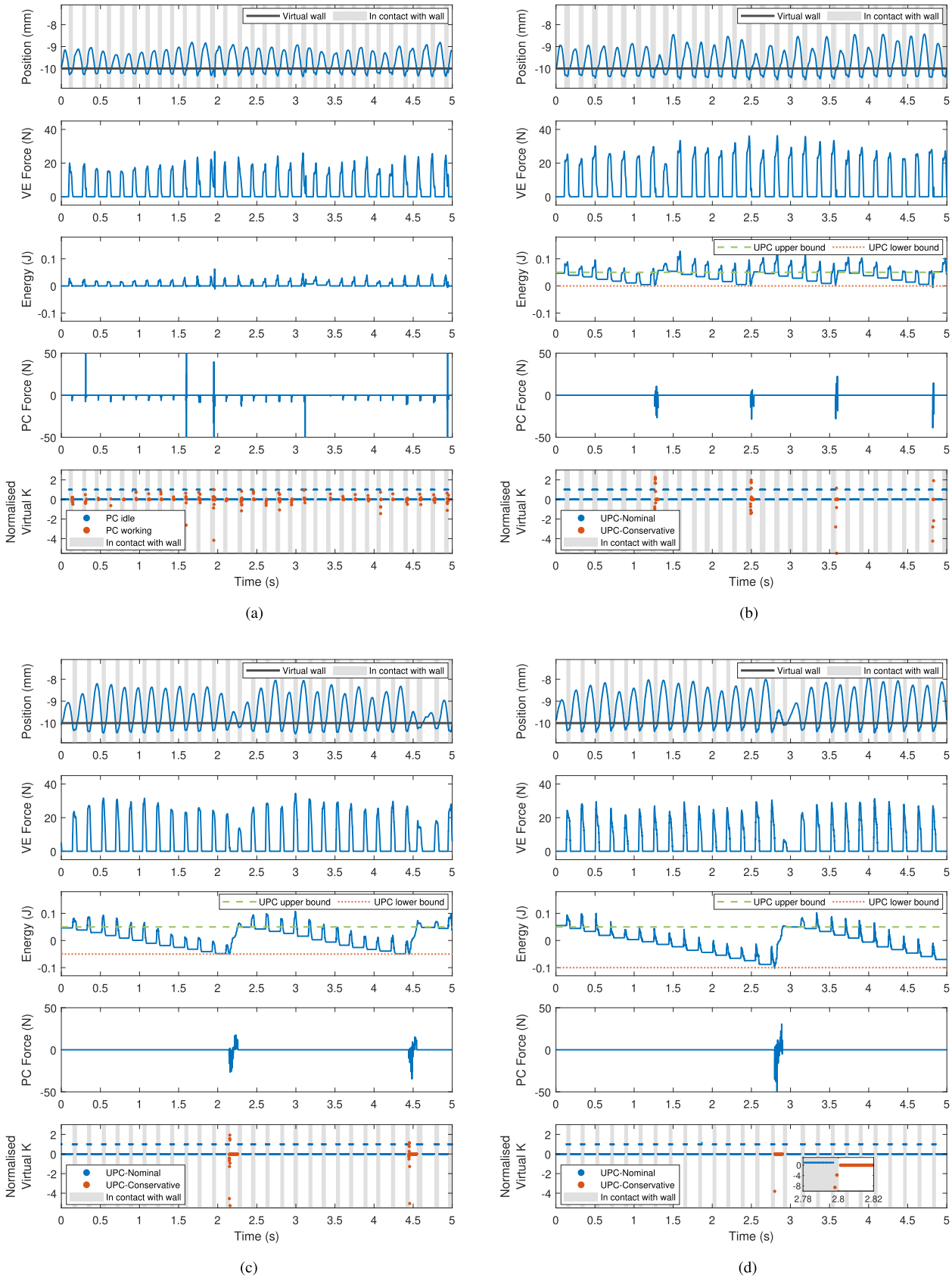

Fig. 12. System performance of the impedance device when the HO held the device end-effector and performed repeated contacts with the virtual wall, under the conditions of (a) the classic PC proposed by [14], and (b) to (d) the proposed UPCs with virtual damping $b_{PC,C} = 60\,\mathrm{Ns}\cdot\mathrm{m}^{-1}$ and lower bound of energy $-\underline{E} = 0\,\mathrm{J}$, $-\underline{E} = -0.05\,\mathrm{J}$, and $-\underline{E} = -0.1\,\mathrm{J}$, respectively. The inserted graph in (d) shows the normalized effective virtual stiffness values outside the y-axis limit. (a) Classic PC. (b) UPC with $-\underline{E} = 0\,\mathrm{J}$. (c) UPC with $-\underline{E} = -0.05\,\mathrm{J}$. (d) UPC with $-\underline{E} = -0.1\,\mathrm{J}$.

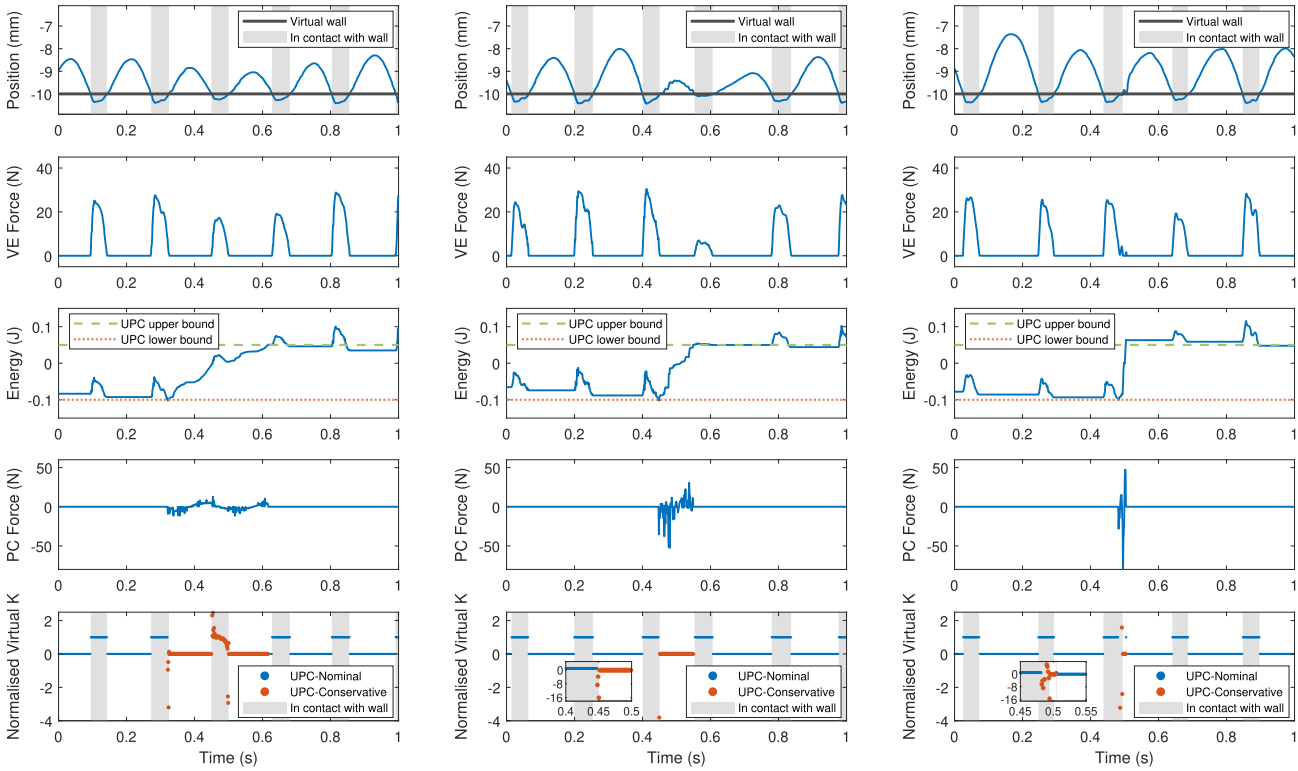

Fig. 13. System performance of the impedance device when the HO held the device end-effector and performed repeated contacts with the virtual wall, under the conditions of (a) to (c) the proposed UPCs with lower bound of energy $-\underline{E} = -0.1\,\mathrm{J}$ and virtual damping $b_{PC,C} = 20\,\mathrm{Ns}\cdot\mathrm{m}^{-1}$, $b_{PC,C} = 60\,\mathrm{Ns}\cdot\mathrm{m}^{-1}$, and $b_{PC,C} = 100\,\mathrm{Ns}\cdot\mathrm{m}^{-1}$, respectively. The inserted graphs in (b) and (c) show the normalized effective virtual stiffness values outside the *y*-axis limit. (a) UPC with $b_{PC,C} = 20\,\mathrm{Ns}\cdot\mathrm{m}^{-1}$. (b) UPC with $b_{PC,C} = 60\,\mathrm{Ns}\cdot\mathrm{m}^{-1}$. (c) UPC with $b_{PC,C} = 100\,\mathrm{Ns}\cdot\mathrm{m}^{-1}$.

the UPC sacrificed stiffness for a much lower number of contacts (only four contacts among 27) when it was setup with a configuration very similar to the classic PC. The UPC was thus able to uphold the system's stability with a smaller cost to the system's performance. Such behavior can be desirable in applications where high fidelity to the VE is expected and only rarely sacrificed, such as in haptic exploration.

By reflecting on the UPC's transient dynamics shown in the experimental results, it can be summarized that the UPC approach is more suitable when challenging environments and rendering behavior are more frequent or continuous. This is more typically the case for admittance-based devices intending to be very transparent while the operator may exhibit high stiffness frequently. In those conditions, the UPC will regularly allow some short nonpassive transient behaviors and compromise performance heavily at a given time, as such providing an overall better rendering of the desired VE over the entire duration of the interaction.

B. *Effects of Delay and Other Nonlinearities*

Similar to the classic PO-PC approach, the UPC relies on a PO to online estimate the energy and determine the PC reactions (i.e., the switching of two control modes in the UPC case). Both of these approaches thus suffer from energy estimation errors due to delays and other nonlinearities [6]. However, the online calculation of a stabilizing virtual damper (as in the classic PO-PC approach) is also strongly affected by control loop delays, which are common in commercial devices.

This is clearly seen in Section V-B where, even if the classic PC was triggered as expected, it was not able to stabilize. This delay leads the PC-produced velocity to be out of phase with the interaction force, compromising the online-calculated PC velocity supposed to stabilize the system. This limitation affecting the classic PC online calculation is clearly exemplified by the control loop delay, but also represents the effect of other nonlinearities in the system.

Although the UPC does not depend on an online calculation of a virtual damper value like the classic PO-PC approach, this delay still influences the timing at which the UPC switches to react, so potentially limiting the UPC performance to some extent. Still, the quasi-constant conservative controller of the UPC does not suffer from the control loop delay and other nonlinearities, hence being able to stabilize the system at the condition to include a reasonable additional stabilizing mass in order to slow down the system. This result also confirms the importance of virtual inertia in stabilizing a delayed admittance-based system.

In real-world implementations, it is possible that a device may not have sufficiently fast sampling or direct measurements of force and velocity signals at the interaction point using fast sensors to provide an accurate energy estimation. In addition, engineers might lack knowledge of the exact delays (if any) in

the system. A reasonably accurate energy estimation by a PO thus cannot be guaranteed, given that the PO's performance is inherently limited by delays and other nonlinearities. In such cases, engineers may consider implementing a robot oscillation detector, as described in [25], to utilize the manifestation of physical phenomena (i.e., oscillation) to determine the timing of switching as compensation for the inaccuracies in the PO.

C. UPC Parameters Tuning

It should also be noted that the UPC scheme has the capability to be applied to different applications by allowing to balance more finely stability and performance based on the exact need. This can be achieved by tuning the virtual damping and energy-bound factors appropriately, effectively balancing how often and how much the controller will sacrifice performance to guarantee stability. As shown in the experimental results of Section VI-C, with a fixed virtual damping and upper bound of energy, selecting a more negative lower bound of energy allows less frequent performance sacrifice while keeping the system ultimately passive. In addition, with a fixed upper bound and lower bound of energy, selecting a larger UPC virtual damping can realise a shorter but heavier performance sacrifice. While illustrated on an impedance device, similar guidelines apply to an admittance device, and the reader can also refer to [40] for a detailed simulation analysis.

As a general guide for UPC parameters selection, if more occasional and heavier performance sacrifices are favoured, a more negative energy lower bound and larger virtual damping should be used, and vice versa.

Furthermore, although it is acknowledged that adding a virtual mass and/or virtual spring element in UPC may assist with system stabilization (usually for admittance-causality), only a small virtual mass was used in the UPC conservative controller configuration for the admittance experiment (see Section V)–as implemented in [25]–while stiffness was omitted as a tradeoff between effective system stabilization and more intuitive and simpler parameter tuning.

D. Limitations

While the proposed UPC approach provides the advantages to: 1) allow transient nonpassive behaviors (so sacrifice the intended behavior less frequently); and 2) allow a more application-specific behavior design of the interaction (i.e., how often and how heavily the PC responds) than previous approaches, the latter advantage also constitutes one of its limitations. Although general guidelines exist to tune the UPC energy bounds and controllers (as illustrated in Section VI-C), no absolute rule can be provided to select such parameters. Thus, the proposed approach appears suitable in scenarios where it is possible to experimentally evaluate the effect of the parameters in order to obtain the best possible behavior for the application.

Finally, it also acknowledged that all experiments presented were run by an HO. While this experimental design has the advantage of demonstrating close to real-world pHRI scenarios, it remains dependent on the repeatability of the HO behavior. Indeed, even if the HO attempted to maintain a very similar interaction behavior for different trials to the best of their ability, this might still introduce some deviations in the approach speed, the HO exerted force and their exhibited stiffness. Future work could use another device to manipulate the robot to mimic the HO in a controlled manner for a more systematic and quantitative evaluation.

VIII. Conclusion

This article proposes a novel concept of ultimate passivity to balance the tradeoff between system performance and stability in pHRI. Compared to traditional passivity-based approaches, this ultimate passivity concept allows the system to have bounded nonpassive transients while ensuring the system is ultimately passive in steady-state. Using such a concept, the UPC is proposed and designed as a switch between a nominal controller for implementing desired performance and a conservative controller for stabilizing the system. Experiments are conducted on admittance-based and impedance-based systems to evaluate the efficacy of the UPC. The experimental results show the capability of UPC in stabilizing the system and maintaining an overall better performance than other approaches, as well as the possibility of defining the balance between performance and stability by appropriate UPC parameter selection.

References

[1] M. Selvaggio, M. Cognetti, S. Nikolaidis, S. Ivaldi, and B. Siciliano, "Autonomy in physical human-robot interaction: A brief survey," *IEEE Robot. Automat. Lett.*, vol. 6, no. 4, pp. 7989–7996, Oct. 2021.

[2] B. D. Argall and A. G. Billard, "A survey of tactile human-robot interactions," *Robot. Auton. Syst.*, vol. 58, no. 10, pp. 1159–1176, 2010.

[3] J. Fong et al., "Promoting clinical best practice in a user-centred design study of an upper limb rehabilitation robot," *Disabil. Rehabil.: Assistive Technol.*, vol. 17, no. 5, pp. 531–538, 2022.

[4] A. Cherubini, R. Passama, A. Crosnier, A. Lasnier, and P. Fraisse, "Collaborative manufacturing with physical human–robot interaction," *Robot. Comput.- Integr. Manuf.*, vol. 40, pp. 1–13, 2016.

[5] N. Hogan, "Impedance control: An approach to manipulation: Part I-theory," *J. Dyn. Syst., Meas. Control, Trans. ASME*, vol. 107, no. 1, pp. 1–7, 1985.

[6] A. Q. L. Keemink, H. van der Kooij, and A. H. A. Stienen, "Admittance control for physical human–robot interaction," *Int. J. Robot. Res.*, vol. 37, no. 11, pp. 1421–1444, 2018.

[7] R. Gillespie and M. R. Cutkosky, "Stable user-specific haptic rendering of the virtual wall," in *Proc. ASME Int. Mech. Eng. Congr. Exhib.*, 1996, vol. 58, pp. 397–406.

[8] B. E. Miller, J. E. Colgate, and R. A. Freeman, "Guaranteed stability of haptic systems with nonlinear virtual environments," *IEEE Trans. Robot. Automat.*, vol. 16, no. 6, pp. 712–719, Dec. 2000.

[9] S. P. Buerger and N. Hogan, "Relaxing passivity for human-robot interaction," in *Proc. 2006 IEEE/RSJ Int. Conf. Intell. Robots Syst.*, 2006, pp. 4570–4575.

[10] S. P. Buerger and N. Hogan, "Complementary stability and loop shaping for improved human–robot interaction," *IEEE Trans. Robot.*, vol. 23, no. 2, pp. 232–244, Apr. 2007.

[11] P. G. Griffiths and R. B. Gillespie, "Recovering haptic performance by relaxing passivity requirements," in *Proc. World Haptics 2009-3rd Joint EuroHaptics Conf. Symp. Haptic Interfaces Virtual Environ. Teleoperator Syst.*, 2009, pp. 326–331.

[12] B. Lacevic and P. Rocco, "Closed-form solution to controller design for human-robot interaction," *J. Dyn. Syst., Meas., Control*, vol. 133, no. 2, 2011, Art. no. 024501.

[13] B. Hannaford and J.-H. Ryu, "Time-domain passivity control of haptic interfaces," *IEEE Trans. Robot. Automat.*, vol. 18, no. 1, pp. 1–10, Feb. 2002.

[14] J.-H. Ryu, Y. S. Kim, and B. Hannaford, "Sampled- and continuous-time passivity and stability of virtual environments," *IEEE Trans. Robot.*, vol. 20, no. 4, pp. 772–776, Aug. 2004.

[15] D. Lee and K. Huang, "Passive-set-position-modulation framework for interactive robotic systems," *IEEE Trans. Robot.*, vol. 26, no. 2, pp. 354–369, Apr. 2010.
[16] J.-P. Kim, S.-y. Baek, and J. Ryu, "A force bounding approach for stable haptic interaction," in *Proc. 2011 IEEE World Haptics Conf.*, 2011, pp. 397–402.
[17] J.-P. Kim, S.-Y. Baek, and J. Ryu, "A force bounding approach for multi-degree-of-freedom haptic interaction," *IEEE/ASME Trans. Mechatron.*, vol. 20, no. 3, pp. 1193–1203, Jun. 2015.
[18] S.-Y. Baek, S. Park, and J. Ryu, "Force bounding approach for stable haptic interaction with dynamic virtual environments," in *Proc. 2017 IEEE Int. Conf. Adv. Intell. Mechatron.*, 2017, pp. 34–39.
[19] J.-P. Kim and J. Ryu, "Robustly stable haptic interaction control using an energy-bounding algorithm," *Int. J. Robot. Res.*, vol. 29, no. 6, pp. 666–679, 2010.
[20] S. Park, R. Uddin, and J. Ryu, "Stiffness-reflecting energy-bounding approach for improving transparency of delayed haptic interaction systems," *Int. J. Control, Automat. Syst.*, vol. 14, no. 3, pp. 835–844, 2016.
[21] F. Ferraguti, C. Secchi, and C. Fantuzzi, "A tank-based approach to impedance control with variable stiffness," in *Proc. 2013 IEEE Int. Conf. Robot. Automat.*, 2013, pp. 4948–4953.
[22] F. Ferraguti et al., "An energy tank-based interactive control architecture for autonomous and teleoperated robotic surgery," *IEEE Trans. Robot.*, vol. 31, no. 5, pp. 1073–1088, Oct. 2015.
[23] C. Schindlbeck and S. Haddadin, "Unified passivity-based cartesian force/impedance control for rigid and flexible joint robots via task-energy tanks," in *Proc. 2015 IEEE Int. Conf. Robot. Automat.*, 2015, pp. 440–447.
[24] A. Dietrich, X. Wu, K. Bussmann, C. Ott, A. Albu-Schaffer, and S. Stramigioli, "Passive hierarchical impedance control via energy tanks," *IEEE Robot. Automat. Lett.*, vol. 2, no. 2, pp. 522–529, Apr. 2017.
[25] F. Ferraguti et al., "A variable admittance control strategy for stable physical human–robot interaction," *Int. J. Robot. Res.*, vol. 38, no. 6, pp. 747–765, 2019.
[26] M. Franken, S. Stramigioli, S. Misra, C. Secchi, and A. Macchelli, "Bilateral telemanipulation with time delays: A two-layer approach combining passivity and transparency," *IEEE Trans. Robot.*, vol. 27, no. 4, pp. 741–756, Aug. 2011.
[27] N. Piccinelli and R. Muradore, "A passivity-based bilateral teleoperation architecture using distributed nonlinear model predictive control," in *Proc. 2020 IEEE/RSJ Int. Conf. Intell. Robots Syst.*, 2020, pp. 11466–11472.
[28] N. Piccinelli and R. Muradore, "A bilateral teleoperation with interaction force constraint in unknown environment using non linear model predictive control," *Eur. J. Control*, vol. 62, pp. 185–191, 2021.
[29] F. Loschi, N. Piccinelli, D. Dall'Alba, R. Muradore, P. Fiorini, and C. Secchi, "An optimized two-layer approach for efficient and robustly stable bilateral teleoperation," in *Proc. 2021 IEEE Int. Conf. Robot. Automat.*, 2021, pp. 12449–12455.
[30] P. Xia, "New advances for haptic rendering: State of the art," *Vis. Comput.*, vol. 34, no. 2, pp. 271–287, 2018.
[31] K. Salisbury, F. Conti, and F. Berbagli, "Haptic rendering: Introductory concepts," *IEEE Comput. Graph. Appl.*, vol. 24, no. 2, pp. 24–32, Mar./Apr. 2004.
[32] H. K. Khalil, *Nonlinear Systems*, 3rd ed. Englewood Cliffs, NJ, USA: Prentice Hall, 2002.
[33] D. Nešić, A. R. Teel, and P. V. Kokotović, "Sufficient conditions for stabilization of sampled-data nonlinear systems via discrete-time approximations," *Syst. Control Lett.*, vol. 38, no. 4-5, pp. 259–270, 1999.
[34] J. Colgate and G. Schenkel, "Passivity of a class of sampled-data systems: Application to haptic interfaces," in *Proc. 1994 Amer. Control Conf.*, 1994, pp. 3236–3240.
[35] J. Zhang and C. C. Cheah, "Passivity and stability of human-robot interaction control for upper-limb rehabilitation robots," *IEEE Trans. Robot.*, vol. 31, no. 2, pp. 233–245, Apr. 2015.
[36] D. Lawrence, "Stability and transparency in bilateral teleoperation," *IEEE Trans. Robot. Automat.*, vol. 9, no. 5, pp. 624–637, Oct. 1993.
[37] J. Colgate and J. Brown, "Factors affecting the Z-width of a haptic display," in *Proc. 1994 IEEE Int. Conf. Robot. Automat.*, 1994, pp. 3205–3210.
[38] J. Fong et al., "CANopen robot controller (CORC): An open software stack for human robot interaction development," *Biosyst. Biorobot.*, vol. 27, 2022, pp. 287–292.
[39] J. Meuleman, E. van Asseldonk, G. van Oort, H. Rietman, and H. van der Kooij, "LOPES II—design and evaluation of an admittance controlled gait training robot with shadow-leg approach," *IEEE Trans. Neural Syst. Rehabil. Eng.*, vol. 24, no. 3, pp. 352–363, Mar. 2016.
[40] Z. Liu, "Balancing performance of haptic physical human-robot interaction," Masters Research thesis, University of Melbourne, Parkville, VIC, Australia, 2022. [Online]. Available: https://minerva-access.unimelb.edu.au/

Xinliang Guo (Student Member, IEEE) received the B.E. degree in electrical engineering from Central South University, China, in 2017, and the M.E. degree in electrical engineering and the M.Phil. degree in rehabilitation engineering, in 2020 and 2023, respectively, from The University of Melbourne, Australia, where he is currently working toward the Ph.D. degree in assistive robotics with the Human Robotics Laboratory, Department of Mechanical Engineering.

His research interests include physical human–robot interaction and robot-assisted rehabilitation.

Zheyu Liu received the B.S. degree in electrical engineering and automation from the Nanjing University of Science and Technology, Nanjing, China, in 2014, and the M.S. degree in electrical and electronic engineering and the M.Phil. degree in intelligent robot force control (research) in 2018 and 2022, respectively, from The University of Melbourne, Australia, where he is currently working toward the Ph.D. degree in robotics with the Human Robotics Laboratory.

From 2021 to 2024, he served as Co-Founder and CTO with Aura Intelligent Control Technology Company, Ltd., focusing on wind energy power optimization, leading strategic development, product promotion, and external collaborations, and overseeing large-scale technology deployment projects. His research interests include stable force control of physical human–robot interaction, visual-based simultaneous localization and mapping, real-time robot perception, and robust autonomous navigation in dynamic environments.

Vincent Crocher received the Master of Engineering degree in electrical engineering and the Ph.D. in robotics from Pierre et Marie Curie University, Paris, France, in 2008 and 2012, respectively.

After a short postdoctoral research fellowship with the Hand Rehabilitation Lab, University of Wisconsin-Milwaukee (USA), he became a Research Fellow with the University of Melbourne (Australia) in 2013. His research interests are in the development and evaluation of tools for physical Human-Robot Interaction and the use of robotics for neurorehabilitation.

Ying Tan (Fellow, IEEE) received the bachelor's degree in electrical engineering from Tianjin University, Tianjin, China, in 1995, and the Ph.D. degree in electrical engineering from the National University of Singapore, Singapore, in 2002.

She is a Professor in mechanical engineering with The University of Melbourne, Melbourne, Australia, specializing in intelligent systems, nonlinear control, data-driven optimization, rehabilitation robotics, and human motor learning. She did a postdoctoral fellowship with McMaster University, Hamilton, Canada, before joining The University of Melbourne in 2004. Her research interests include control theory, artificial intelligence, and human-centered robotics, with significant contributions to rehabilitation robotics, wearable sensors, and intelligent optimization methods for complex dynamical systems.

Dr. Tan is the recipient of several prestigious fellowships, including an Australian Postdoctoral Fellowship (2006–2008) and an ARC Future Fellowship (2009–2013). She currently serves on the ARC College of Experts (2024–2026) and is a Fellow of Engineers Australia and the Asia-Pacific Artificial Intelligence Association. She is also an IEEE Fellow Committee member (2024–2025) and a Distinguished Lecturer for the IEEE Control Systems Society.

Denny Oetomo (Senior Member, IEEE) received the Ph.D. degree in robotics from the National University of Singapore, Singapore, in 2004.

He conducted postdoctoral research with Monash University, Melbourne, Australia, and INRIA Sophia-Antipolis, France. In 2008, he joined The University of Melbourne, Melbourne, where he is currently a Professor with the Department of Mechanical Engineering. His research interests include robotic manipulation and human–robot interaction, with applications in assistive and rehabilitation robotics.

Arno H. A. Stienen received the M.Sc. degree in mechanical engineering from the Delft University of Technology, Delft, The Netherlands, in 2003, and the Ph.D. degree in rehabilitation robotics from the University of Twente, Enschede, The Netherlands, in 2009.

He was a specialist in human–machine interaction, exoskeletons, and robotics in unstructured and compliant environments, his expertise lies in biomechatronics and human–robot interaction, particularly for rehabilitation and industrial support. He was an Associate Professor with the University of Twente, Enschede, The Netherlands, and Northwestern University, Evanston, IL, USA, until 2016. His academic contributions include the Freebal rehabilitation robot (later Hocoma ArmeoBoom) and SaeboMAS. In 2016, he transitioned to industry, leading rehabilitation robotics at Motek Medical BV, later becoming Director and VP Product Management with DIH Rehabilitation Solutions. He oversaw product launches, including the Motek RYSEN and Hocoma ArmeoSenso. In 2020, he joined DEMCON Advanced Mechatronics, focusing on robotic systems in medical, industrial, and agricultural fields. In 2022, he returned to academia as an Associate Professor with TU Delft's Biomechanical Engineering department, applying industry insights to advance human supportive devices.